

## ANGULAR MOMENTUM TRANSPORT AND PROTON–ALPHA-PARTICLE DIFFERENTIAL STREAMING IN THE SOLAR WIND

Bo Li

Institute of Mathematical and Physical Sciences, University of Wales, Aberystwyth SY23 3BZ, UK; bbl@aber.ac.uk

SHADIA RIFAI HABBAL

Institute for Astronomy, University of Hawaii, Honolulu, HI 96822

AND

XING LI

Institute of Mathematical and Physical Sciences, University of Wales, Aberystwyth SY23 3BZ, UK

Received 2006 December 29; accepted 2007 February 12

### ABSTRACT

The interplay between the proton–alpha-particle differential flow speed,  $v_{\alpha p}$ , and angular momentum transport in the solar wind is explored by using a three-fluid model. The force introduced by the azimuthal components is found to play an important role in the force balance for ions in interplanetary space, bringing the radial flow speeds of protons and alpha particles closer to each other. For the fast solar wind, the model cannot account for the decrease of  $v_{\alpha p}$  observed by *Helios* between 0.3 and 1 AU. However, it can reproduce the  $v_{\alpha p}$  profile measured by *Ulysses* beyond 2 AU, if the right value for  $v_{\alpha p}$  is imposed at that distance. In the slow wind, the effect of solar rotation is more pronounced if one starts with the value measured by *Helios* at 0.3 AU: a relative change of 10%–16% is introduced in the radial speed of the alpha particles between 1 and 4 AU. The model calculations show that, although alpha particles consume only a small fraction of the energy and linear momentum fluxes of protons, they cannot be neglected when considering the proton angular momentum flux  $L_p$ . In most examples, it is found that  $L_p$  is determined by  $v_{\alpha p}$  for both the fast and the slow wind. In the slow solar wind, the proton and alpha particle angular momentum fluxes  $L_p$  and  $L_\alpha$  can be several times larger in magnitude than the flux carried by the magnetic stresses  $L_M$ . While the sum  $L_p = L_p + L_\alpha$  is smaller than  $L_M$ , for the modeled fast and slow wind alike, this result is at variance with the *Helios* measurements.

*Subject headings:* solar wind — Sun: magnetic fields

### 1. INTRODUCTION

The relative velocity between protons and alpha particles in the solar wind,  $v_{\alpha p} \equiv v_\alpha - v_p$ , offers important clues for understanding the mechanisms responsible for the solar wind acceleration. In the fast solar wind with proton speeds  $v_p = |v_p| \gtrsim 600 \text{ km s}^{-1}$ , *Helios* measurements made in near-ecliptic regions indicate that there exists a substantial  $v_{\alpha p} = |v_{\alpha p}| \text{sign}(v_\alpha - v_p)$ , which may be  $150 \text{ km s}^{-1}$  at the heliocentric distance  $r \approx 0.3 \text{ AU}$ , amounting to  $\sim 1/4$  of the local proton speed. This  $v_{\alpha p}$  decreases with increasing  $r$  to  $30\text{--}40 \text{ km s}^{-1}$  at 1 AU. Furthermore, for a continuous high-latitude fast stream sampled by *Ulysses* between 1995 May and 1996 August, it was found that the average  $v_{\alpha p}$  decreases from  $\sim 40 \text{ km s}^{-1}$  at 1.5 AU to  $\sim 15 \text{ km s}^{-1}$  at 4.2 AU (Reisenfeld et al. 2001). As for the slow stream with  $v_p \lesssim 400 \text{ km s}^{-1}$ ,  $v_{\alpha p}$  tends to be zero on average (see Marsch et al. 1982 and references therein). However, as clearly shown by Figure 11 in Marsch et al. (1982), there seem to be two categories of slow solar winds: in one alpha particles tend to flow faster than protons, whereas in the other this tendency is reversed. That  $v_{\alpha p} \approx 0$  therefore reflects the fact that the two kinds of slow winds have nearly equal opportunities to be present. Marsch et al. (1982) interpreted  $v_{\alpha p} > 0$  as a consequence of the wave acceleration that favors alpha particles and  $v_{\alpha p} < 0$  as a signature of the solar wind being driven primarily by the electrostatic field since alpha particles experience only half the electric force that protons do. The former interpretation has been corroborated by an example on day 117 of 1978, during which period there existed simultaneously strong Alfvén wave activities, as well as a significant positive  $v_{\alpha p}$  at  $r \approx 0.29 \text{ AU}$ . This  $v_{\alpha p}$  ( $\sim 100 \text{ km s}^{-1}$ ) is 20%–30% of the measured proton speed (Marsch et al. 1981).

*Helios* measurements have also yielded information concerning the angular momentum transport in the solar wind, in particular, the distribution of the angular momentum loss  $L$  between particles  $L_p$  and magnetic stresses  $L_M$ , and the further partition of  $L_p$  between protons  $L_p$  and alpha particles  $L_\alpha$  (Pizzo et al. 1983; Marsch & Richter 1984). In spite of the significant scatter, the data nevertheless exhibit a distinct trend for  $L_p$  to be positive (negative) for solar winds with proton speeds  $v_p$  below (above)  $400 \text{ km s}^{-1}$ . The precise measurement of  $L_\alpha$  is even more difficult; however, on average  $L_\alpha$  displays a tendency similar to that of  $L_p$ . The magnetic contribution  $L_M$ , on the other hand, is remarkably constant. A mean value of  $L_M = 1.6 \times 10^{29} \text{ dynes cm sr}^{-1}$  can be quoted for the solar winds of all flow speeds and throughout the region from 0.3 to 1 AU. For comparison, the mean values of angular momentum fluxes carried by ion flows in the slow solar wind are  $L_p = 19.6$  and  $L_\alpha = 1.3 \times 10^{29} \text{ dynes cm sr}^{-1}$  (see Table II of Pizzo et al. 1983). The fluxes carried by all particles is then  $L_p = L_p + L_\alpha = 20.9 \times 10^{29} \text{ dynes cm sr}^{-1}$ , which tends to be larger than  $L_M$ . It should be noted that, such a value for  $L_p$  corresponds to an azimuthal speed of more than  $7 \text{ km s}^{-1}$  for the bulk slow wind, consistent with the measurements made before the *Helios* era (see the data compiled in § I of Pizzo et al. 1983).

The aforementioned problems are not isolated from each other. As a matter of fact, it has been shown that in the presence of solar rotation, an additional force appears in the meridional momentum equation of minor ion species. The effect of this force is to bring the meridional speed of minor ions to that of protons (McKenzie et al. 1979; Hollweg & Isenberg 1981). It is noteworthy that when using the azimuthal speed of minor ions, McKenzie et al. (1979) were mainly concerned with deriving the

so-called rotational force rather than the angular momentum transport. Hence, the azimuthal proton speed was neglected altogether. Hollweg & Isenberg (1981) offered a more convenient and more self-consistent derivation of that force by working in the corotating frame; however, the azimuthal dynamics was again neglected. An extension to the study of McKenzie et al. (1979) has been recently given by Li & Li (2006, hereafter Paper I), who worked in the inertial frame and, in improvement of McKenzie et al. (1979) treated the protons and alpha particles on an equal footing. The resulting model is in effect a three-fluid version of the model of Weber & Davis (1967). A low-latitude, fast solar wind solution was worked out, and it was shown that the solar rotation introduces a barely perceptible difference in the profiles of the meridional ion speeds within 1 AU. However, the proton–alpha-particle differential streaming plays a decisive role in determining the azimuthal speeds, and thus the individual angular momentum fluxes, of not only alpha particles but also protons.

Li & Li's (2006) model was restricted to the region within 1 AU and gave only one solution for the purpose of presenting a general analysis of the angular momentum transport in a three-fluid solar wind. In this study we explore, in a quantitative and systematic manner, the interplay between the angular momentum transport and proton–alpha-particle differential streaming in both the slow and fast solar wind for the region extending from the coronal base out to 4.5 AU. It should be noted that so far the only available measurements of the alpha-particle angular momentum flux are from *Helios*, which explored the near-ecliptic solar wind between 0.3 and 1 AU (Pizzo et al. 1983; Marsch & Richter 1984). The *Helios* measurements will therefore be compared with the computed ion angular momentum fluxes for the region within 1 AU only. The numerical results for the region outside 1 AU will concern only the proton–alpha-particle differential streaming  $v_{\alpha p}$ , therefore allowing a comparison of  $v_{\alpha p}$  with the *Ulysses* measurements.

Before proceeding, we note that several mechanisms have been proposed to account for the observed evolution of the proton–alpha-particle differential speed  $v_{\alpha p}$  in the fast solar wind beyond 0.3 AU. Since they have been critically reviewed in the introduction section of Kaghshvili et al. (2003) some brief remarks are sufficient here. First, the ponderomotive force due to Alfvén waves tends to limit  $|v_{\alpha p}|$ , but it operates too slowly to reduce  $v_{\alpha p}$  in the observed manner, especially in the region between 0.3 and 1 AU. Second, various microinstabilities, in particular, the magnetosonic one, are expected to be operational when they have a threshold of  $v_{\alpha p}$  of order the local Alfvén speed. However, these microinstabilities are more likely to be effective in regions beyond 1 AU where the parallel proton beta is large. For a more comprehensive review of these kinetic aspects, please see Marsch (2006). Third, the compressional waves accompanying large-amplitude Alfvén waves may help convert the free energy that derives from the differential streaming into alpha-particle heating, thereby reducing  $v_{\alpha p}$  (Kaghshvili et al. 2003). Finally, although intuitively appealing, the Coulomb friction proves inefficient for regulating  $v_{\alpha p}$  in the majority of the solar wind measured by *Helios*. It may play some role only for the relatively dense slow wind when  $|v_{\alpha p}| \lesssim 15 \text{ km s}^{-1}$  (see Figs. 13 and 15 in Marsch et al. 1982). The functional dependence on  $|v_{\alpha p}|$  of the Coulomb collision frequency between protons and alpha particles, contained in the coefficient  $c_0$  in equation (1), dictates that the friction force will rapidly decrease rather than increase with increasing  $|v_{\alpha p}|$  if  $|v_{\alpha p}|$  exceeds a critical value. Except for the Coulomb friction, the aforementioned mechanisms are not included in the present study as we try to isolate the effect of solar rotation on the evo-

lution of  $v_{\alpha p}$ , since it is an inherent process whose existence is independent of the wave processes. We further note that the effect of solar rotation has been incorporated in a number of three-fluid solar wind models (e.g., Isenberg & Hollweg 1983; Bürgi & Geiss 1986; Hu & Habbal 1999). However, in all these papers, the spiral magnetic field is assumed rather than computed, and the azimuthal speeds of ions are neglected. These models are therefore not suitable for our purpose, i.e., to examine the angular momentum transport in a three-fluid solar wind.

The paper is organized as follows. We first give a brief overview of the model in § 2. Some further details on the numerical implementation of the model are given in § 3. Then § 4 presents the numerical results, which are summarized in § 5.

## 2. PHYSICAL MODEL

The solar wind model consists of three species, electrons ( $e$ ), protons ( $p$ ), and alpha particles ( $\alpha$ ). Each species  $s$  ( $s = e, p, \alpha$ ) is characterized by its density  $n_s$ , velocity  $\mathbf{v}_s$ , mass  $m_s$ , electric charge  $e_s$ , and temperature  $T_s$ . The electric charge is also measured in units of electron charge  $e$ , i.e.,  $e_s = Z_s e$ , with  $Z_e \equiv -1$  by definition. The ion mass number  $A_k$  follows from the relation  $m_k = A_k m_p$  ( $k = p, \alpha$ ). The mass density of species  $s$  is  $\rho_s = n_s m_s$ , and the species partial pressure is  $p_s = n_s k_B T_s$ , where  $k_B$  is the Boltzmann constant. From quasi-neutrality it follows that  $n_e = n_p + Z_\alpha n_\alpha$ . We also assume quasi-zero-current, i.e.,  $\mathbf{v}_e = (n_p \mathbf{v}_p + Z_\alpha n_\alpha \mathbf{v}_\alpha) / n_e$ , except when the ion momentum equations are derived. The governing equations, which self-consistently take into account the effect of solar rotation, are identical to those in Paper I and will not be given here. They are appropriate for a time-independent solar wind assuming azimuthal symmetry, i.e.,  $\partial/\partial\phi \equiv 0$  in a heliocentric spherical coordinate system ( $r, \theta, \phi$ ). In what follows, we will describe briefly the model, with the emphasis on the possible effects introduced by the azimuthal components. In addition, we will also give an analysis of the distribution of the total angular momentum flux between the magnetic field and particles.

### 2.1. Model Description

It was shown in the appendix of Paper I that no mass or energy exchange between different flux tubes is possible, thereby allowing the system of equations to be expressed as a force balance condition across the poloidal magnetic field coupled with the conservation equations along it. In this study, the force balance condition is replaced by prescribing a radial (i.e., perfectly monopolar) magnetic field. The model equations can therefore be solved for the radial distribution of the densities  $n_k$  and radial speeds  $v_{kr}$  of ion species ( $k = p, \alpha$ ), the temperatures  $T_s$  of all species ( $s = e, p, \alpha$ ), as well as the azimuthal components of the magnetic field  $B_\phi$  and ion velocities  $v_{k\phi}$ . As such, the model can be seen as a 1.5-dimensional (1.5D) one in that the only independent variable is the heliocentric distance  $r$  and, however, both the radial and azimuthal components of vectors are retained. To illustrate the effects of solar rotation, we will also compute models without the  $\phi$ -components. For the ease of description these models will be called 1D. Furthermore, the ion heat fluxes are neglected, and the field-aligned electron heat flux  $\mathbf{q}_e$  is assumed to follow the Spitzer law, which results in  $\nabla \cdot \mathbf{q}_e = -(1/a)(\partial/\partial r)[a\kappa T_e^{5/2}(\partial T_e/\partial r) \cos^2\Phi]$ . Here the cross-sectional area of the flux tube  $a$  scales as  $a \propto 1/B_r \propto r^2$ , and the magnetic azimuthal angle  $\Phi$  is defined by  $\tan \Phi = B_\phi/B_r$ . As for the electron conductivity  $\kappa$ , the Spitzer value is used,  $\kappa = 7.8 \times 10^{-7} \text{ ergs K}^{-7/2} \text{ cm}^{-1} \text{ s}^{-1}$  (Spitzer 1962).

From Paper I, the equation governing the radial speed of ion species  $k$  is

$$v_{kr} \frac{\partial v_{kr}}{\partial r} = -\frac{1}{n_k m_k} \frac{\partial p_k}{\partial r} - \frac{Z_k}{n_e m_k} \frac{\partial p_e}{\partial r} - \frac{GM_\odot}{r^2} + a_k + \frac{n_j}{A_k n_e} c_0 (v_{jr} - v_{kr}) \sec^2 \Phi + \left[ \frac{v_{k\phi}^2}{r} - \tan \Phi v_{kr} \left( \frac{\partial v_{k\phi}}{\partial r} + \frac{v_{k\phi}}{r} \right) \right], \quad (1)$$

where the subscript  $j$  denotes the species other than  $k$ , i.e.,  $j = \alpha$  for  $k = p$  and vice versa, and  $c_0$  is a coefficient associated with Coulomb frictions. Moreover,  $G$  is the gravitational constant,  $M_\odot$  is the mass of the Sun, and  $a_k$  stands for the acceleration from some external process. Apart from  $a_k$ , the meridional acceleration of the ion flow includes the ion and electron pressure gradient forces (the terms proportional to  $\partial p_k/\partial r$  and  $\partial p_e/\partial r$ , respectively), the gravitational force, the Coulomb friction corrected for the spiral magnetic field, and the force associated with azimuthal flow speeds (the term in the brackets, hereafter referred to as the ‘‘azimuthal force’’ for brevity). Note that the electron pressure gradient force is part of the electrostatic force, which is apportioned between two ion species according to their charge-to-mass ratios  $Z_k/A_k$  ( $k = p, \alpha$ ).

Introducing  $\phi$ -components impacts the meridional dynamics through two means. First, the electron conductivity is in effect reduced by a factor of  $\cos^2 \Phi$ , thereby affecting the electron temperature and hence the electron pressure gradient force. Second, the azimuthal force enters into the meridional momentum equations. The two effects can both be important, as will be illustrated by the numerical solutions presented in § 4.2.

## 2.2. Angular Momentum Loss Rate and Its Distribution between Particles and Magnetic Stresses

In what follows, a simple analysis based on constants of motion for the governing equations shows how the angular momentum loss rate per steradian  $L$  is distributed between particles  $L_P$  and magnetic stresses  $L_M$  in a solar wind where different ion species flow with different velocities. As such, this discussion complements that of Weber & Davis (1967) and Marsch & Richter (1984) where the solar wind is seen as a bulk flow.

Following Paper I, the expressions for the azimuthal components  $v_{p\phi}$ ,  $v_{\alpha\phi}$ , and  $B_\phi$  are

$$v_{p\phi} = \frac{\Omega r \sin \theta}{M_T^2 - 1} \left[ \overbrace{M_T^2 \frac{r_A^2}{r^2} - 1}^{\text{I}} + \overbrace{M_\alpha^2 \frac{v_{\alpha p, r}}{v_{\alpha r}} \left( 1 - \frac{r_A^2}{r^2} \right)}^{\text{II}} \right], \quad (2a)$$

$$v_{\alpha\phi} = \frac{\Omega r \sin \theta}{M_T^2 - 1} \left[ \overbrace{M_T^2 \frac{r_A^2}{r^2} - 1}^{\text{I}} + \overbrace{M_p^2 \frac{v_{\alpha p, r}}{v_{pr}} \left( \frac{r_A^2}{r^2} - 1 \right)}^{\text{II}} \right], \quad (2b)$$

$$B_\phi = \Omega r \sin \theta \frac{4\pi \rho_p v_{pr} (1 + \zeta) r_A^2 / r^2 - 1}{B_r M_T^2 - 1}, \quad (2c)$$

where  $v_{\alpha p, r}$  is the radial component of the velocity difference vector  $\mathbf{v}_{\alpha p}$ ,  $\Omega$  is the angular rotation rate of the flux tube, and the constant  $\zeta = (\rho_\alpha v_{\alpha r})/(\rho_p v_{pr})$  denotes the ion mass flux ratio. The terms designated by II are associated with the differential streaming, whereas the terms denoted by I take care of the rest. The

subscript A denotes the Alfvénic point where  $M_T = 1$ ,  $M_T$  being the combined meridional Alfvénic Mach number defined by

$$M_T^2 = M_p^2 + M_\alpha^2, \quad M_k^2 = \frac{v_{kr}^2}{B_r^2 / 4\pi \rho_k}, \quad (3)$$

with  $k = p, \alpha$ .

The field and particle contributions to the angular momentum loss rate per steradian  $L$  are

$$L_M = -r^3 \sin \theta \frac{B_\phi B_r}{4\pi}, \quad L_k = r^3 \sin \theta \rho_k v_{kr} v_{k\phi}, \quad (4)$$

where  $k = p, \alpha$ . From equations (2a)–(2c) it follows that

$$L = \dot{M} \Omega r_A^2 \sin^2 \theta, \quad (5)$$

where  $\dot{M} = (1 + \zeta) \rho_p v_{pr} r^2$  is the total mass-loss rate of the solar wind. The ratio  $L_k/L_M$  is rather complex and had better be examined case by case due to the presence of terms labeled II in equations (2a) and (2b). Note that terms II derive essentially from the requirement that the proton–alpha-particle velocity difference vector be aligned with the instantaneous magnetic field (Li & Li 2006). The azimuthal speeds are expected to be determined by these terms when there exists a substantial  $v_{\alpha p, r}$ , which is almost exclusively determined by the way in which the external energy is distributed among different species in the corona. As shown in § 4, such a situation happens for the majority of the numerical solutions in interplanetary space. Hence, the azimuthal speeds and the resulting specific angular momenta of ion species measured in situ are essentially determined by the processes that happen in the corona. Furthermore, it follows from the identity  $\rho_p v_{pr} M_\alpha^2 / v_{\alpha r} = \rho_\alpha v_{\alpha r} M_p^2 / v_{pr}$  that terms II have no contribution to the overall angular momentum loss rate. As a result, a concise result can be found for the ratio of the overall particle contribution  $L_P = L_p + L_\alpha$  to the magnetic one  $L_M$ . By defining the bulk velocity

$$\mathbf{u} = (\mathbf{v}_p + \zeta \mathbf{v}_\alpha) / (1 + \zeta), \quad (6)$$

one can see  $M_T^2 = (r/r_A)^2 (u_r/u_{r,A})$ . As a result,

$$\frac{L_P}{L_M} = \frac{u_r/u_{r,A} - 1}{1 - r_A^2/r^2}. \quad (7)$$

It is interesting to see that only one single speed  $u_r$  enters into the ratio  $L_P/L_M$ .

In comparison with Weber & Davis (1967) and Marsch & Richter (1984) the expressions here indicate that a proper definition of the Alfvénic point is through  $M_T = 1$  and the bulk flow velocity  $\mathbf{u}$  should be defined as an average between the proton and alpha-particle velocities, weighted by their respective mass fluxes (cf. eq. [6]). Of course these differences only matter when the abundance of alpha particles and the differential streaming between the protons and the alpha particles are large. When  $\zeta = 0$  or  $\mathbf{v}_\alpha = \mathbf{v}_p$ , the results are identical to those in Marsch & Richter (1984).

## 3. NUMERICAL IMPLEMENTATION

The model has been briefly described in § 2 where a rather general analysis is also given. However, it is still necessary to solve the governing equations numerically for a quantitative analysis to be made. In particular, some external heating and/or momentum addition need to be applied to the ions to generate a

TABLE 1  
PARAMETERS CHARACTERIZING THE ENERGY DEPOSITION TO ION SPECIES

Wind Type	$F_E$ (ergs cm <sup>-2</sup> s <sup>-1</sup> )	$l_d$ ( $R_\odot$ )	$\chi$	$\chi_d$
Fast.....	1.8	5	1.8	... <sup>a</sup>
Slow.....	1.2	1	2.9	0

<sup>a</sup> The parameter  $\chi_d$  decreases with  $r$  from 30 to 1 with a sharp transition at  $2 R_\odot$ .

solar wind solution. The implementation of the energy deposition and a description of the method of solution are given in this section.

### 3.1. Energy Deposition

The external energy deposition is assumed to come from an ad hoc energy flux that dissipates at a constant length  $l_d$ . The resulting total heating rate is therefore

$$Q = F_E \frac{B_r}{B_{rE} l_d} \exp\left[-\frac{(r - R_\odot)}{l_d}\right],$$

where  $F_E$  is the input flux scaled to the Earth orbit  $R_E = 1$  AU,  $B_{rE} = 3.3\gamma$  is the radial magnetic field strength at  $R_E$ , and  $R_\odot$  is the solar radius. The energy is deposited in protons entirely as heat  $Q_p$  but deposited in the alpha-particle gas in the form of both heating  $Q_\alpha$  and acceleration  $a_\alpha$ . To be more specific,  $Q$  is apportioned among  $Q_p$ ,  $Q_\alpha$ , and  $a_\alpha$  in the following way,

$$Q_p + \bar{Q}_\alpha = Q, \quad \frac{\bar{Q}_\alpha}{Q_p} = \frac{\chi \rho_\alpha}{\rho_p}, \quad (8a)$$

$$Q_\alpha + \rho_\alpha v_{\alpha r} a_\alpha = \bar{Q}_\alpha, \quad \frac{a_\alpha}{Q_\alpha} = \frac{\chi d}{\rho_\alpha v_0}, \quad (8b)$$

where  $v_0 = (k_B T_p / m_p)^{1/2}$  is some characteristic speed.

The choice of the heat and momentum deposition needs some explanation. The exponential form of  $Q$  was first suggested by Holzer & Axford (1970) and was later employed in a large number of studies. The form of  $Q$  adopted here is slightly different from the original version to ensure that it mimics the dissipation of a flux of nonthermal energy, for instance, the dissipation of low-frequency Alfvén waves. This may happen as a result of a turbulent cascade toward high parallel wavenumbers where the wave energy is picked up by ions through the ion-cyclotron resonance. (For more details, please see the review by Hollweg & Isenberg [2002] dedicated to this topic.) Once  $Q$  is specified, the way it is distributed among different ion species, characterized by the parameter  $\chi$ , depends on the resonant interaction between cyclotron waves and ions. Note that  $\chi$  indicates how alpha particles are favored when  $Q$  is distributed, with  $\chi = 1$  standing for the neutral heating: the total energy that goes to ion species  $k$  is proportional to its mass density  $\rho_k$  ( $k = p, \alpha$ ). Previous computations involving ion cyclotron waves indicate that, in the case of neutral heating, the alpha particles tend to flow slower than protons (see the dispersionless case in Fig. 1 of Hu & Habbal 1999). Only when the alpha particles are energetically favored in the corona can the modeled  $v_{\alpha p}$  be positive in interplanetary space. This happens when  $\chi > 1$ . (Note that we adopted a constant  $\chi$  throughout the computational domain for simplicity.) Listed in Table 1, and unless otherwise stated, the heating parameters are chosen to produce fast or slow solar wind solutions with realistic ion mass fluxes and terminal speeds.

### 3.2. Method of Solution and Boundary Conditions

The governing equations (eqs. [1]–[7] in Paper I) are cast in a time-dependent form and are solved by using a fully implicit numerical scheme (Hu et al. 1997). Starting from an arbitrary guess, the equations are advanced in time until a steady state is reached. The computational domain extends from the coronal base ( $1 R_\odot$ ) to 4.5 AU. At the base, the ion densities and species temperatures are fixed,  $n_e = 3 \times 10^8$  cm<sup>-3</sup>,  $n_\alpha/n_p = 0.1$ ,  $T_e = T_p = T_\alpha = 1.2 \times 10^6$  K. The radial components of ion velocities,  $v_{pr}$  and  $v_{\alpha r}$ , are specified to ensure mass conservation. On the other hand,  $v_{p\phi}$  and  $B_\phi$  are specified according to equations (2a)–(2c). At the outer boundary (4.5 AU), all dependent variables are linearly extrapolated for simplicity. We take  $\Omega = 2.865 \times 10^{-6}$  rad s<sup>-1</sup>, which corresponds to a sidereal rotation period of 25.38 days.

## 4. NUMERICAL RESULTS

As has been described in § 1, we are interested in answering two questions: (1) To what extent is  $v_{\alpha p}$ , the differential streaming between protons and alpha particles, affected by introducing solar rotation? and (2) Is it possible to reconcile the model results with the *Helios* measurements, as far as the specific angular momentum fluxes are concerned? In this section, we will first examine the fast solar wind and then move on to the slow one.

### 4.1. Fast Solar Wind Solutions

#### 4.1.1. Effect of Solar Rotation on the Differential Streaming

A comparison of the 1.5D (*solid curves*) with the 1D model (*dotted curves*) of the fast solar wind solution in the equatorial plane (colatitude  $\theta = 90^\circ$ ) is given in Figure 1. Plotted are the radial profiles for (a) the radial component of the proton–alpha-particle velocity difference  $v_{\alpha p,r}$ , and (b) the radial ion speeds  $v_{pr}$  and  $v_{\alpha r}$ . In Figure 1a, the dash-dotted line shows the parameter  $v_{\alpha p} = v_{\alpha p,r} \sec \Phi$ , which also takes into account the azimuthal component of the difference vector. The asterisk denotes the Alfvénic point in the 1.5D model, which lies at  $r_A = 12.6 R_\odot$ . For comparison, the open boxes give the near-ecliptic *Helios* measurements of  $v_{\alpha p}$  for the fast wind as reported by Marsch et al. (1982).

From Figures 1a and 1b, one can see that introducing the solar rotation only affects the solar wind beyond, say,  $50 R_\odot$ . Thus, it is not surprising that the ion fluxes are unchanged in the 1.5D model, as compared with the 1D one. Both models yield an ion flux ratio of  $(n_\alpha v_{\alpha r})/(n_p v_{pr}) = 0.026$  and a proton flux of  $(n_p v_{pr})_E = 2.72 \times 10^8$  cm<sup>-2</sup> s<sup>-1</sup> when scaled to 1 AU.

It can be seen from Figure 1a that, although  $v_{\alpha p,r}$  decreases with radial distance  $r$  for both the 1D and 1.5D models beyond their mutual maximum of 147 km s<sup>-1</sup> attained at  $9.4 R_\odot$ , the reduction in  $v_{\alpha p,r}$  is more prominent in the 1.5D model from 0.3 to 4 AU. The reduction in  $v_{\alpha p}$  for the 1.5D model, when compared with the 1D one, is also substantial, although less significant than the reduction in  $v_{\alpha p,r}$  due to the presence of the azimuthal component of  $v_{\alpha p}$ . Nevertheless, the 1.5D model yields a  $v_{\alpha p}$  of 11.4 km s<sup>-1</sup> at 4 AU, as opposed to 29.3 km s<sup>-1</sup> attained in the 1D model. From Figure 1b one can see that the reduction in  $v_{\alpha p,r}$  in the 1.5D model is achieved by lowering the radial speed profile of alpha particles  $v_{\alpha r}$  and raising that of protons  $v_{pr}$ . This effect is barely perceptible at 0.3 AU but becomes more obvious with increasing  $r$ .

Figure 1a indicates that the modeled  $v_{\alpha p}$  profile deviates significantly from the *Helios* measurements, especially in the region closer to the Sun. In other words, the deceleration of alpha

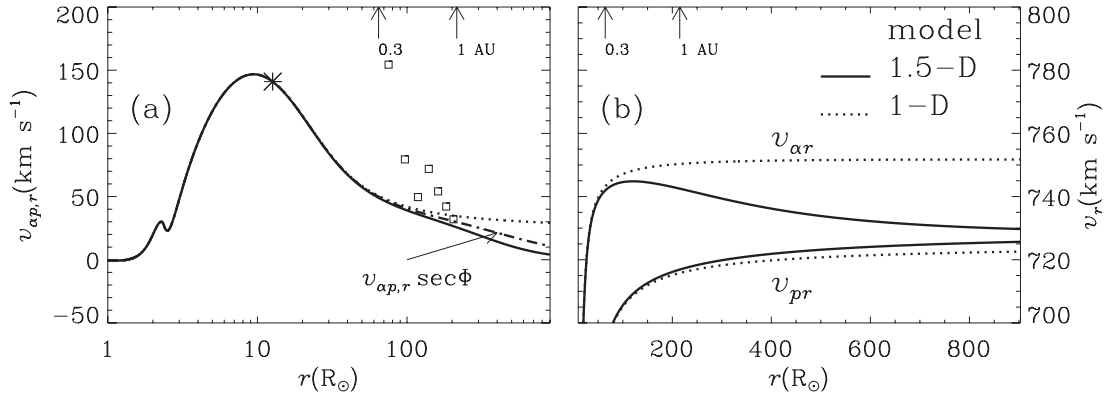


FIG. 1.— Effect of solar rotation on a three-fluid fast solar wind in the equatorial plane  $\theta = 90^\circ$ . The azimuthal components of ion velocities and the magnetic field are incorporated self-consistently in the 1.5D model (solid curves), but excluded in the 1D model (dotted curves). Radial profiles are shown for several flow parameters: (a) the radial component of the proton–alpha-particle relative velocity  $v_{\alpha p} = v_\alpha - v_p$  and (b) the radial speeds of protons  $v_{pr}$  and alpha particles  $v_{\alpha r}$ . In (a),  $v_{\alpha p} = v_{\alpha p,r} \sec \Phi$  is given by the dash-dotted line, where  $\Phi$  is the magnetic azimuthal angle, defined by  $\tan \Phi = B_\phi/B_r$ . The asterisk refers to the Alfvénic point where  $M_T = 1$ ,  $M_T$  being the combined Alfvénic Mach number defined by eq. (3). In addition, the squares give the near-ecliptic *Helios* measurements of  $v_{\alpha p}$  reported by Marsch et al. (1982).

particles relative to protons as measured by *Helios* cannot be explained by merely invoking the  $\phi$ -components. However, can this mechanism be entirely ruled out as far as the *Ulysses* measurements are concerned? Such a possibility is examined in Figure 2. In Figure 2a, the distribution of  $v_{\alpha p}$  in the  $r$ - $\theta$  plane for the region extending from 1 to 4.2 AU is displayed as contours equally spaced by  $1 \text{ km s}^{-1}$ . The solutions are obtained by varying the colatitude  $\theta$  alone. Recalling that by assumption the solar wind flows in a perfectly monopolar magnetic field, one may see that the latitudinal dependence is entirely due to solar rotation. From Figure 2a it is obvious that in the regions close to the pole, say  $\theta \lesssim 10^\circ$ ,  $v_{\alpha p}$  shows little radial dependence. However, with increasing  $\theta$ , the radial gradient in  $v_{\alpha p}$  becomes increasingly significant.

In Figure 2b, the solid curve represents the modeled  $v_{\alpha p}$  profile along the *Ulysses* trajectory delineated by the dashed curve in Figure 2a in the interval between 1995 May 5 and 1996 August 2. During this period, *Ulysses* sampled a continuous, undisturbed, high-speed stream above the latitude of  $N30^\circ$  in the radial range of  $\sim 1.5$ –4.2 AU. The actual *Ulysses* measurements are

given by the error bars, which correspond to the 25%–75% percentiles of the  $v_{\alpha p}$  distribution over 10 day bins (Reisenfeld et al. 2001). It can be seen that, for  $r \lesssim 2 \text{ AU}$ ,  $v_{\alpha p}$  in the numerical solutions increases as opposed to the observed tendency for  $v_{\alpha p}$  to decrease. This is because during this period, *Ulysses* was moving toward the pole, and the effect of solar rotation diminishes with decreasing  $\theta$ . However, for  $r \gtrsim 2 \text{ AU}$ , the decrease in  $v_{\alpha p}$  from  $30.7 \text{ km s}^{-1}$  at 2 AU to  $12.4 \text{ km s}^{-1}$  at 4.2 AU is consistent with the observed values within the accuracy of the measurements. From this we conclude that solar rotation should not be neglected in attempts to understand the *Ulysses* measurements of  $v_{\alpha p}$  beyond 2 AU. It is necessary to stress that this conclusion should not be confused with that reached by Reisenfeld et al. (2001), who demonstrated by showing a profile designated “*Ulysses* rotational deceleration” in their Figure 8 that the  $v_{\alpha p}$  profile measured by *Ulysses* has little to do with the rotational deceleration. In fact, we agree with these authors that introducing solar rotation cannot provide a unified mechanism to account for the observed deceleration of  $v_{\alpha p}$  from 0.3 AU onward. What

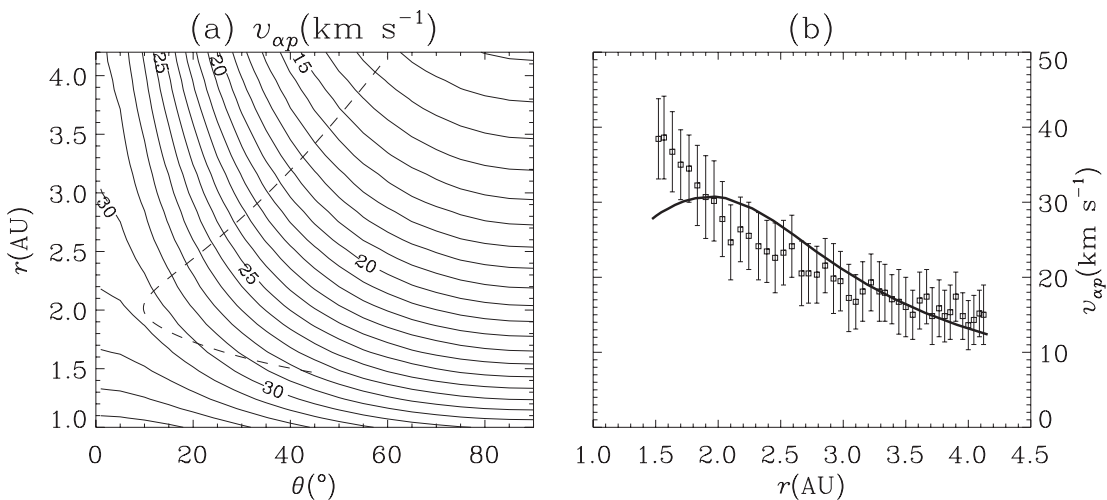


FIG. 2.— Effect of solar rotation on a three-fluid fast solar wind. (a) Distribution in the  $r$ - $\theta$  plane of the proton–alpha-particle differential speed  $v_{\alpha p}$  for the region extending from 1 to 4.2 AU. The contours are equally spaced by  $1 \text{ km s}^{-1}$ . The dashed line depicts the trajectory of *Ulysses* in the interval between 1995 May 5 and 1996 August 2. The solutions are obtained by varying the colatitude  $\theta$  alone with all other parameters unchanged. As such, the latitudinal dependence of  $v_{\alpha p}$  is entirely due to solar rotation. (b) Radial profile of the modeled  $v_{\alpha p}$  along the *Ulysses* trajectory (solid line). The error bars represent 25%–75% of the  $v_{\alpha p}$  distribution over 10 day bins as sampled by *Ulysses* (Reisenfeld et al. 2001).

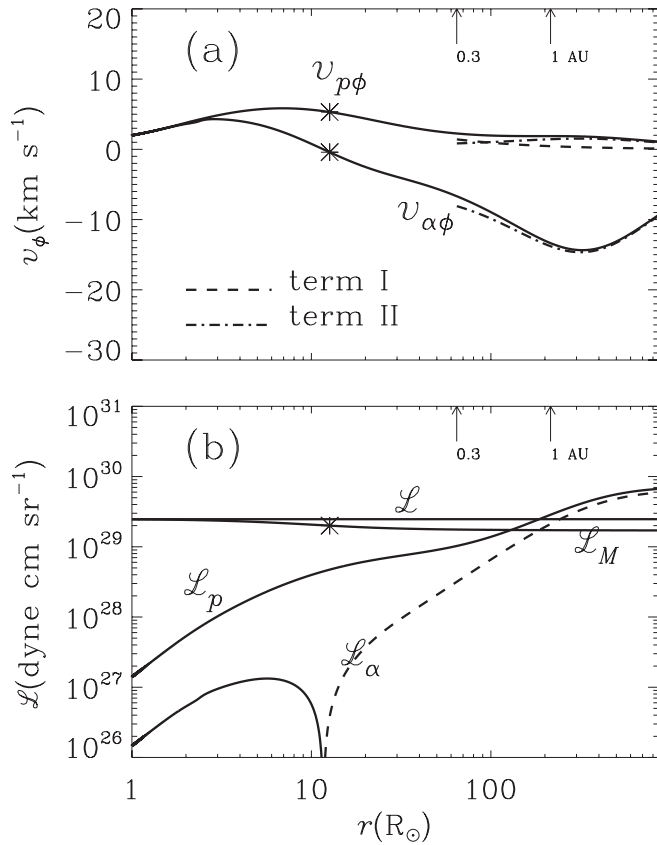


FIG. 3.— Angular momentum transport in a three-fluid fast solar wind. (a) Azimuthal speeds of protons  $v_{p\phi}$  and alpha particles  $v_{\alpha\phi}$ , and (b) specific angular momentum fluxes carried by protons  $L_p$ , alpha particles  $L_{\alpha}$ , and magnetic stresses  $L_M$ . The fluxes add up to  $L$ . In (a), the dashed line shows the contribution from term I in eqs.(2a) and (2b), whereas the dash-dotted curves give the contribution from term II. In (b), the dashed line represents negative values. The asterisks mark the position of the Alfvénic point  $r_A$ .

Figure 2b shows is that, if a reasonable  $v_{\alpha p}$  is given at 2 AU, the solar rotation alone can decelerate the alpha particles relative to protons in the observed fashion.

#### 4.1.2. Angular Momentum Transport

We now turn to the problem of the angular momentum transport in the fast solar wind along  $\theta = 90^\circ$ . Figure 3 describes the radial distribution of (a) the azimuthal ion speeds  $v_{p\phi}$  and  $v_{\alpha\phi}$ , and (b) the specific angular momentum fluxes including those carried by protons  $L_p$ , alpha particles  $L_{\alpha}$ , and magnetic stresses  $L_M$ . The total angular momentum flux  $L$  should be a constant, as is indeed the case in the numerical solution. To isolate the contribution of the differential streaming to individual azimuthal speeds, term I (II) in equations (2a) and (2b) is plotted as the dashed (dash-dotted) curve between 0.3 and 4 AU. In Figure 3b, the dashed line is used for plotting negative values. The asterisks in both panels mark the Alfvénic point  $r_A$ .

From Figure 3a one can see that with the development of  $v_{\alpha p, r}$ , some substantial difference arises between  $v_{p\phi}$  and  $v_{\alpha\phi}$ . To be more specific,  $v_{p\phi}$  increases from the coronal base to  $5.84 \text{ km s}^{-1}$  at  $6.9 R_{\odot}$ , beyond which  $v_{p\phi}$  decreases gradually to  $1.1 \text{ km s}^{-1}$  around 4 AU. On the other hand,  $v_{\alpha\phi}$  reaches a local maximum of  $4.3 \text{ km s}^{-1}$  at  $2.88 R_{\odot}$ . Rather than partially corotate with the Sun, alpha particles then gradually develop an azimuthal velocity in the direction of counterrotation with the Sun:  $v_{\alpha\phi}$  is negative beyond  $11.7 R_{\odot}$ . Then  $v_{\alpha\phi}$  attains a local minimum of  $-14.4 \text{ km s}^{-1}$  at  $324 R_{\odot}$  and increases thereafter to  $-9.35 \text{ km s}^{-1}$  at 4 AU. It

can be seen that, for  $r \geq 0.3 \text{ AU}$  not only  $v_{\alpha\phi}$  but also  $v_{p\phi}$  are determined mainly by term II (dash-dotted lines) in their respective expressions (2a) and (2b).

Despite the small values of  $v_{p\phi}$ , Figure 3b reveals that  $L_p$  exceeds  $L_M$  in the region beyond  $129 R_{\odot}$ . Furthermore,  $L_{\alpha}$  becomes larger than  $L_M$  in magnitude for  $r \geq 186 R_{\odot}$ . Consider the values at 1 AU. As part of the total flux  $L = 2.47$  (all values are in units of  $10^{29} \text{ dyne cm sr}^{-1}$ ), the magnetic part  $L_M = 1.72$  is smaller than the proton contribution  $L_p = 2.86$ , which, however, is largely offset by the alpha-particle contribution  $L_{\alpha} = -2.12$ . As a matter of fact, magnetic stresses are always the primary constituent in  $L$ ; the particle contribution as a whole is smaller than  $L_M$  throughout the computational domain. At  $1 R_{\odot}$ , 99.37% of  $L$  is contained in magnetic stresses  $L_M$ . Although  $L_M$  decreases monotonically with increasing distance, it still amounts to 69.2% of  $L$  at 4 AU. This is understandable in view of equation (7). For  $r \sim R_{\odot}$ , one can see that  $r \ll r_A$  and  $u_r \ll u_{r,A}$ . It then follows that  $L_M/L \approx 1 - (r/r_A)^2 \approx 1$ . On the other hand, for  $r \gg r_A$  one can see  $L_M/L \approx u_{r,A}/u_r$ . That  $L_M$  takes up most of the total flux  $L$  asymptotically therefore stems from the fact that  $u_{r,A}/u_r$  varies little beyond  $r_A$ .

The value of  $L_M$  (in units of  $10^{29} \text{ dyne cm sr}^{-1}$ ) shows only a slight decrease from 1.76 at 0.3 AU to 1.72 at 1 AU. This is consistent with the quoted value of  $\sim 1.6\text{--}1.9$  as measured by *Helios* (Pizzo et al. 1983; Marsch & Richter 1984). However, *Helios* measurements indicate that in the fast solar wind, both  $L_{\alpha}$  and  $L_p$  tend to be negative. As a result, the overall particle contribution  $L_p$  is negative, which can be realized only if the solar wind bulk speed  $u_r$  decreases with  $r$  in the region  $r \geq r_A$ . This is not possible by simply varying the heating parameters in the model. Instead, we would rather interpret Figure 3 as an indication that the proton angular momentum flux cannot be studied on its own, i.e., by simply incorporating  $\phi$ -components into models of an electron-proton plasma. Although alpha particles take up only a minor part of the solar wind momentum and energy fluxes, the proton-alpha-particle differential speed is the primary contributor to individual azimuthal ion speeds and therefore to individual ion angular momentum fluxes.

#### 4.2. Slow Solar Wind Solutions

The effect of solar rotation on individual ion speeds in the fast solar wind is rather weak inside 1 AU. Is this also the case for the slow wind? Moreover, the *Helios* measurements show that in the slow solar wind, the proton and alpha-particle angular momentum fluxes are both positive. When added together, they are also larger than that carried by magnetic stresses. Can this measurement be explained by the present model? To answer these questions, we will first examine an example with a significant positive  $v_{\alpha p, r}$  to gain some insight. A parameter study surveying the parameter  $\chi$  will then be presented.

##### 4.2.1. Effect of Solar Rotation on the Differential Streaming

Figure 4 compares a 1.5D (solid curves) with 1D model (dotted curves) of the slow solar wind in the equatorial plane  $\theta = 90^\circ$ . Plotted are the radial profiles for (a) the radial component of the proton-alpha-particle velocity difference  $v_{\alpha p, r}$  and (b) the radial speeds of ions  $v_{kr}$  ( $k = p, \alpha$ ). In Figure 4a, the asterisk denotes the Alfvénic point in the 1.5D model, which now lies at  $r_A = 14.2 R_{\odot}$ . The dash-dotted line is used to show the parameter  $v_{\alpha p}$ .

As in the case for the fast wind, introducing the solar rotation does not alter the ion fluxes. When scaled to 1 AU, both the 1D and 1.5D models yield a proton flux of  $(n_p v_{pr})_E = 3.36 \times 10^8 \text{ cm}^{-2} \text{ s}^{-1}$  and a flux ratio of  $(n_{\alpha} v_{\alpha r}) / (n_p v_{pr}) = 0.024$ . Furthermore, introducing the  $\phi$ -components reduces the proton-alpha-particle

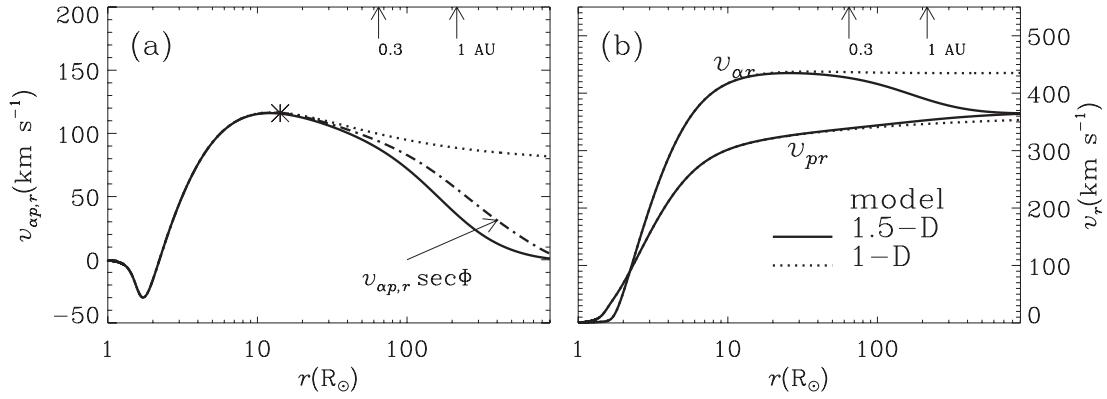


FIG. 4.— Effect of solar rotation on three-fluid slow solar winds in the equatorial plane  $\theta = 90^\circ$ . The 1.5D model is given by solid curves, whereas the 1D one is given by dotted curves. (a) Radial component of the proton–alpha-particle relative velocity  $v_{\alpha p,r}$ , and (b) the radial speeds of protons  $v_{pr}$  and alpha particles  $v_{\alpha r}$ . In (a), the asterisk refers to the Alfvénic point, and the dash-dotted line shows  $v_{\alpha p} = v_{\alpha p,r} \sec \Phi$ .

differential speed by decelerating the alpha particles and accelerating the protons. Take the radial speeds at 1 AU, for instance. The 1.5D model yields  $v_{\alpha r} = 389 \text{ km s}^{-1}$ , whereas the 1D model results in  $v_{\alpha r} = 435 \text{ km s}^{-1}$ . As for  $v_{pr}$ , the 1.5D (1D) model yields 353 (347)  $\text{km s}^{-1}$ . As a result,  $v_{\alpha p,r}$  at 1 AU is 88  $\text{km s}^{-1}$  for the 1D but 36  $\text{km s}^{-1}$  for the 1.5D model. Going further to 4 AU, in the 1D model alpha particles still flow considerably faster than protons: values of  $v_{\alpha r} = 435$  and  $v_{pr} = 353 \text{ km s}^{-1}$  are found at 4 AU. In contrast,  $v_{\alpha r}$  and  $v_{pr}$  attain nearly the same value ( $\sim 365 \text{ km s}^{-1}$ ) in the 1.5D model. It should be noted that, a value of  $v_{\alpha p} = 88 \text{ km s}^{-1}$  at 0.3 AU seen in Figure 4a for the 1.5D model is not unrealistic. Even larger values have been found for  $v_{\alpha p}$  by *Helios 2* when approaching perihelion (Marsch et al. 1981). However,  $v_{\alpha p}$  at 1 AU seems somehow unrealistic; a value of  $56 \text{ km s}^{-1}$  is substantially larger than the local Alfvén speed  $V_A = B_r \sec \Phi / [4\pi(\rho_p + \rho_\alpha)]^{1/2}$ , which yields  $35 \text{ km s}^{-1}$ . By contrast, the *Helios* measurements indicate that in the slow wind the ratio  $v_{\alpha p}/V_A$  spans a broad distribution between  $-1$  and  $1$  but peaks at  $\sim \pm 0.25$  (Fig. 11 in Marsch et al. 1982). The discrepancy indicates once again that invoking the solar rotation alone is not an efficient way to decelerate the alpha particles relative to protons. However, if some yet unknown mechanism results in a substantial  $v_{\alpha p}$  at 0.3 AU as observed, the effect of solar rotation on the evolution of  $v_{\alpha p}$  with radial distance  $r$  beyond 0.3 AU probably cannot be neglected from the perspective of slow solar wind modeling. For instance, in this particular solution, the changes introduced in the alpha-particle speed  $v_{\alpha r}$  at the distance of 4 (1) AU can be 16.1% (10.5%) of the the values in the case without taking solar rotation into account.

Returning to the discussion of  $v_{\alpha p}$ , one may expect that  $v_{\alpha p}$  is largely determined by the proportion of the external energy deposited to alpha particles, characterized by the parameter  $\chi$ . Figure 5 displays the dependence on  $\chi$  of  $v_{\alpha p}$  at several different radial distances as labeled. Results from 1.5D models are displayed by thick curves, whereas those from 1D models are given by thin curves for comparison. Inspection of the solid lines shows that the transition from negative to positive  $v_{\alpha p}$  at 0.3 AU occurs at  $\chi = 1.6$  in both models. With  $\chi$  varying between 0.5 and 3.4,  $v_{\alpha p}$  at 0.3 AU goes from  $-132$  to  $127 \text{ km s}^{-1}$  for the 1.5D model, while it goes from  $-143$  to  $134 \text{ km s}^{-1}$  for the 1D model. When comparing the thin and thick solid lines, one can see that the profile of  $v_{\alpha p}$  for 1D models differs only slightly from that for 1.5D ones. Going from 0.3 to 4 AU, the magnitude of  $v_{\alpha p}$  is significantly reduced by introducing the azimuthal components. Unsurprisingly this effect is more prominent at the high and low ends. For instance the 1D model for  $\chi = 3.4$  yields  $v_{\alpha p} = 120 \text{ km s}^{-1}$

at 4 AU, whereas the corresponding 1.5D model gives  $v_{\alpha p} = 21.8 \text{ km s}^{-1}$ . It turns out that introducing the  $\phi$ -components reduces  $v_{\alpha p}$  via different mechanisms for different portions of this parameter range. For  $\chi$  between 1.0 and 2.3, the proton–alpha-particle friction eventually becomes operative between 0.3 and 4 AU to suppress any significant  $|v_{\alpha p}|$ . As a result, no obvious deviation shows up between 1D and 1.5D models. If  $\chi \gtrsim 2.3$ , the reduction of  $|v_{\alpha p}|$  in the 1.5D model is achieved partly by the enhanced electron pressure gradient force (which stems from the enhanced electron temperature due to reduced effective electron thermal conductivity in presence of the spiral field) and more importantly via the azimuthal force. On the other hand, for  $\chi \lesssim 1$ , the reduction in  $|v_{\alpha p}|$  is solely due to the azimuthal force, since in this case, the electron pressure–gradient force tends to increase the magnitude of  $v_{\alpha p}$  as a consequence of the smaller charge-to-mass ratio of alpha particles compared with that of protons.

#### 4.2.2. Angular Momentum Transport

Figure 6 displays the distribution with  $\chi$  of the values at 1 AU of (a) the azimuthal speeds of ions  $v_{p\phi}$  and  $v_{\alpha\phi}$ , and (b) specific angular momentum fluxes including that carried by protons  $L_p$ , alpha particles  $L_\alpha$ , as well as by magnetic stresses  $L_M$ . From Figure 6a one can see that  $v_{p\phi}$  and  $v_{\alpha\phi}$  at 1 AU tend to have opposite signs, evidence that they are mainly determined by the terms associated with  $v_{\alpha p,r}$  in equations (2a) and (2b). As a matter of fact, for all  $\chi$  but  $\chi = 1.9$ , term II in equation (2b) contributes more than term I to  $v_{\alpha\phi}$ . As for  $v_{p\phi}$ , with the exception of  $1.4 \leq \chi \leq 2$ ,

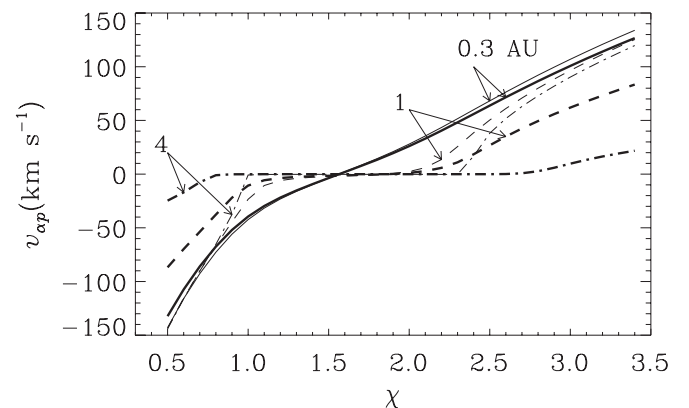


FIG. 5.— Dependence of the proton–alpha-particle differential speed  $v_{\alpha p}$  on the parameter  $\chi$  at three radial distances, as labeled, for the 1.5D model (thick curves) and the 1D one (thin curves).

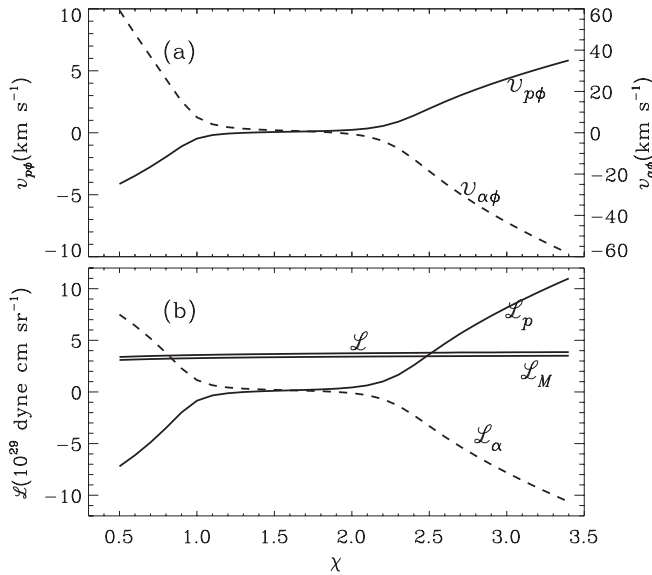


FIG. 6.— Values of several parameters at 1 AU as a function of parameter  $\chi$ : (a) azimuthal speeds of protons  $v_{p\phi}$  and alpha particles  $v_{\alpha\phi}$ , and (b) specific angular momentum fluxes carried by the proton fluid  $L_p$ , the alpha-particle fluid  $L_\alpha$ , and magnetic stresses  $L_M$ . The total flux  $L$  is also given.

the main contribution also comes from term II in equation (2a). Looking at Figure 5, one finds that for this narrow range of  $\chi$ ,  $v_{\alpha p}$  at 1 AU ranges from  $-3$  to  $1.1 \text{ km s}^{-1}$ . At substantial relative speeds between protons and alpha particles,  $v_{p\phi}$  can become as large as  $5.84 \text{ km s}^{-1}$  when  $\chi = 3.4$ , for which  $v_{\alpha\phi} = -58.5 \text{ km s}^{-1}$ . At the other extreme  $\chi = 0.5$ ,  $v_{p\phi}$  ( $v_{\alpha\phi}$ ) is  $-4.1$  ( $59.3$ )  $\text{km s}^{-1}$ . In addition, from Figure 6b one can see that  $L_M$  or  $L$  varies little, although  $L_p$  and  $L_\alpha$  vary significantly within the parameter range as a consequence of the sensitive dependence of  $v_{\alpha\phi}$  and  $v_{p\phi}$  on  $\chi$ . For instance, when  $\chi$  varies from 0.5 to 3.4,  $L$  shows only a slight increase from  $3.39$  to  $3.86 \times 10^{29}$  dynes  $\text{cm sr}^{-1}$ , and  $L_M$  increases from  $3.09$  to  $3.51 \times 10^{29}$  dynes  $\text{cm sr}^{-1}$ . The increase of  $L$  with  $\chi$  can be explained by equation (5). For the solutions considered, the location of the Alfvénic point varies little. However, the mass-loss rate, which is mainly determined by the proton flux, increases with increasing  $\chi$  as a consequence of more energy being deposited to the subsonic portion for the proton gas (Leer & Holzer 1980). On the other hand, the ratio  $L_M/L$  shows little variation with  $\chi$ . This can be seen as an indication that the ratio of the bulk speed  $u_r$  attained asymptotically to that at the Alfvénic point is rather insensitive to  $\chi$ , since  $L_M/L \approx u_{r,A}/u_r$  in the region  $r \gg r_A$  (cf. eq. [7]). Moreover, if  $u_r$  varies little beyond  $r_A$ , as is the case for all the obtained slow wind solutions,  $L_M/L$  should be only slightly less than unity for  $r \gg r_A$ . The expectation is reproduced by Figure 6b, from which one can see that magnetic stresses are always the most important term in  $L$ , despite the fact that individual angular momentum fluxes carried by ion species,  $L_p$  or  $L_\alpha$ , can be much larger than  $L_M$ .

Now the model results can be compared with the *Helios* measurements for specific angular momentum fluxes (Pizzo et al. 1983; Marsch & Richter 1984). One can see that, although  $L_M$  falls within the uncertainties of the measurements, and values like  $1.3 \times 10^{29}$  dynes  $\text{cm sr}^{-1}$  can be found for  $L_\alpha$  at  $\chi \approx 1$ , no values as large as  $19.6 \times 10^{29}$  dynes  $\text{cm sr}^{-1}$  can be found for  $L_p$  unless the alpha particles are heated even more intensely. Moreover, Figure 6b does not reproduce the observed tendency for the particle contribution  $L_p$  to be larger than the magnetic one  $L_M$  at 1 AU. As has been discussed, the reason is that the solar wind bulk flow  $u_r$  experiences little acceleration outside the Alfvénic point  $r_A$ . It

is unlikely that this feature can be changed by simply varying other model parameters. Actually the discrepancy between model predictions and measurements on the relative importance of  $L_p$  and  $L_M$  is common to all existing models that treat the meridional and azimuthal dynamics self-consistently (cf. §§ I and VII of Pizzo et al. 1983). To examine the possible sources leading to this discrepancy, in what follows we consider some of the physics that is not accounted for in the present model.

In the framework of steady state models, the fast and slow magnetosonic waves, in the Wentzel-Kramers-Brillouin (WKB) approximation, have nonzero  $r\phi$  components in their stress tensors, thereby also contributing to the angular momentum loss of the solar wind (Marsch 1986). On the one hand, this contribution may be comparable to that due to the background flow and magnetic field stress when the waves have sufficiently large amplitudes. On the other hand, depending on the propagation angle with respect to the background magnetic field, the particle part may dominate the magnetic one in the wave contribution. (This can be seen if one evaluates the  $r\phi$  component of eq. [7] by using, e.g., the fast-wave eigenfunction eq. [10] in Marsch [1986].) Therefore, including compressional waves may provide a possible means to resolve the apparent discrepancy. Furthermore, extending the WKB analysis to higher order, Hollweg (1973) found that Alfvén waves with finite wavelength may carry a nonvanishing flux of angular momentum, but the contribution seems to worsen rather than improve the discrepancy. Finally, we refer the reader to the discussion of Hu et al. (2003) whose 2.5D model also incorporates the momentum deposition by Alfvén waves. Instead of attributing this discrepancy to mechanisms missing in the steady state model, Hu et al. (2003) proposed that the tendency for  $L_p$  to be larger than  $L_M$  is due to interplanetary dynamical processes such as the forward fast shocks traversing the solar wind. Their discussion also applies to the present model, although the details of the response of the three-fluid plasma to fast shocks need to be explored.

## 5. SUMMARY

The near-ecliptic measurements of the fast solar wind by *Helios* demonstrated the existence of a significant proton–alpha-particle differential speed,  $v_{\alpha p}$ , varying from  $150 \text{ km s}^{-1}$  at 0.3 AU to  $30\text{--}40 \text{ km s}^{-1}$  at 1 AU (Marsch et al. 1982). A steady decrease of  $v_{\alpha p}$  between 1.5 and 4 AU was also measured by *Ulysses* out of the ecliptic plane (Reisenfeld et al. 2001). The *Helios* measurements also indicated the existence of two categories of slow solar wind. In one category, the alpha particles tended to be slower than the protons, whereas the opposite trend was found in the other category (Marsch et al. 1982). The measurements also yielded information about the angular momentum transport, in particular, the specific angular momentum fluxes in the magnetic stress  $L_M$ , and in the two major ion species  $L_p$  and  $L_\alpha$  (Pizzo et al. 1983; Marsch & Richter 1984).

In an attempt to account for these observations, we introduced solar rotation self-consistently in a three-fluid solar wind model. The impetus for this approach was inspired by the fact that the solar rotation is an inherent process, independent of different mechanisms invoked for accelerating the solar wind. By exploring the resulting interplay between  $v_{\alpha p}$  and the angular momentum transport, we reached the following conclusions:

1. The force introduced in the radial momentum equations by the azimuthal components can play a significant role in the force balance in interplanetary space. Its main effect is to reduce the difference between the ion flow speeds.
2. While the effect of solar rotation could not account for the decrease in  $v_{\alpha p}$  in the fast solar wind from 0.3 to 1 AU, it could

account for the  $v_{\alpha p}$  profile measured by *Ulysses* beyond 2 AU if an appropriate value for  $v_{\alpha p}$  was chosen at 2 AU.

3. The effect of solar rotation was found to be more pronounced for the slow solar wind if a significant  $v_{\alpha p}$  developed by 0.3 AU, resulting in a relative change of 10%–16% in the radial speed of the alpha particles between 1 and 4 AU.

4. For the slow solar wind solutions considered, the angular momentum flux carried by alpha particles,  $L_{\alpha}$ , at 1 AU, was almost exclusively determined by  $v_{\alpha p}$ . Moreover,  $L_p$  was also determined by  $v_{\alpha p}$  for  $v_{\alpha p} \gtrsim 1$  or  $\lesssim -3$  km s<sup>-1</sup>.

5. In the fast solar wind,  $L_p$  and  $L_{\alpha}$  beyond 0.3 AU are also mainly due to  $v_{\alpha p}$ . This suggests that even though alpha particles take up only a small fraction of the energy and linear momentum fluxes of protons, they cannot be neglected when the proton angular momentum flux is concerned, i.e.,  $L_p$  cannot be studied by simply incorporating the azimuthal components into models of an electron-proton solar wind.

6. For the slow solar wind,  $L_p$  and  $L_{\alpha}$  can be several times larger in magnitude than the flux carried by the magnetic stresses  $L_M$ . However, the total particle distribution  $L_P = L_p + L_{\alpha}$  is always smaller than  $L_M$  for all solutions. While this tendency is inherent to the present model, it is at variance with the *Helios* measurements.

In closing, some words of caution seem in order. As has been discussed, a pure fluid model of a quiet solar wind as adopted in this study is rather idealized. In reality, the solar wind will be subject to various disturbances such as compressional magnetosonic waves, shock waves, and other processes resulting from stream-stream interactions. These disturbances may significantly modify the distribution of the angular momentum flux between particles and magnetic field stresses, and may alter the overall angular momentum loss rate of the solar wind. With increasing distance, such as in the outer heliosphere, these disturbances are expected to become increasingly important. With this caveat in mind, the presented study nevertheless provides a better understanding of the underlying physics. Even when the above-mentioned dynamical processes are taken into account, one would expect to see that solar rotation has significant effects on the alpha-particle flow speeds in interplanetary space, and in turn, alpha particles are important in the problem of angular momentum transport of the solar wind.

This work is supported by a PPARC rolling grant to the University of Wales, Aberystwyth. We wish to thank the anonymous referee for the constructive comments that helped improve the manuscript.

#### REFERENCES

- Bürgi, A., & Geiss, J. 1986, *Sol. Phys.*, 103, 347  
 Hollweg, J. V. 1973, *J. Geophys. Res.*, 78, 3643  
 Hollweg, J. V., & Isenberg, P. A. 1981, *J. Geophys. Res.*, 86, 11463  
 ———. 2002, *J. Geophys. Res.*, 107(A7), 12  
 Holzer, T. E., & Axford, W. I. 1970, *ARA&A*, 8, 31  
 Hu, Y. Q., Esser, R., & Habbal, S. R. 1997, *J. Geophys. Res.*, 102, 14661  
 Hu, Y. Q., & Habbal, S. R. 1999, *J. Geophys. Res.*, 104, 17045  
 Hu, Y. Q., Li, X., & Habbal, S. R. 2003, *J. Geophys. Res.*, 108(A10), 9  
 Isenberg, P. A., & Hollweg, J. V. 1983, *J. Geophys. Res.*, 88, 3923  
 Kaghshvili, E. K., Vasquez, B. J., & Hollweg, J. V. 2003, *J. Geophys. Res.*, 108(A1), 8  
 Leer, E., & Holzer, T. E. 1980, *J. Geophys. Res.*, 85, 4681  
 Li, B., & Li, X. 2006, *A&A*, 456, 359 (Paper 1)  
 Marsch, E. 1986, *A&A*, 164, 77  
 Marsch, E. 2006, *Living Rev. Sol. Phys.*, 3, 1, <http://solarphysics.livingreviews.org/Articles/lrsp-2006-1/>  
 Marsch, E., Mühlhäuser, K.-H., Rosenbauer, H., Schwenn, R., & Denskat, K. U. 1981, *J. Geophys. Res.*, 86, 9199  
 Marsch, E., Mühlhäuser, K.-H., Rosenbauer, H., Schwenn, R., & Neubauer, F. M. 1982, *J. Geophys. Res.*, 87, 35  
 Marsch, E., & Richter, A. K. 1984, *J. Geophys. Res.*, 89, 5386  
 McKenzie, J. F., Ip, W.-H., & Axford, W. I. 1979, *Ap&SS*, 64, 183  
 Pizzo, V., Schwenn, R., Marsch, E., Rosenbauer, H., Mühlhäuser, K.-H., & Neubauer, F. M. 1983, *ApJ*, 271, 335  
 Reisenfeld, D. B., Gary, S. P., Gosling, J. T., & Steinberg, T. 2001, *J. Geophys. Res.*, 106, 5693  
 Spitzer, L., Jr. 1962, *Physics of Fully Ionized Gases* (New York: Wiley)  
 Weber, E. J., & Davis, L., Jr. 1967, *ApJ*, 148, 217